JOURNAL OF PROPULSION AND POWER
Vol. 12, No. 1, January–February 1996

Near- and Far-Field Plume Studies of a One-Kilowatt Arcjet

Alec D. Gallimore,* Sang-Wook Kim,† John E. Foster,† Lyon B. King,† and Frank S. Gulczinski III†
University of Michigan, Ann Arbor, Michigan 48109-2118

To support studies of transport in arcjet plumes, axial and radial profiles of electron temperature, electron number density, stagnation pressure, and flowfield were obtained over an extensive volume of the plume of a 1-kW arcjet operating on hydrogen. All experiments were performed in a 6 by 9 m vacuum chamber at a tank pressure of less than 4×10^{-4} torr during arcjet operation. Electron temperatures obtained spectroscopically 1.2 cm downstream of the exit plane ranged from 0.10 to 0.13 eV, while electron number densities determined ~2 cm downstream of the exit plane via langmuir probe varied between $0.3–1 \times 10^{12}$ cm^{-3}. Far-field langmuir probe measurements showed that a rapid radial variation in electron number density exists, ranging from 0.5 to 5×10^{9} cm^{-3}, and from 0.5 to 2×10^{9} cm^{-3}, 30 and 88 cm downstream of the exit plane, respectively. Electron temperatures at these axial locations show much less of an axial dependence, ranging between 0.07–0.20 eV at both axial positions. Finally, an impact pressure probe was used to measure the radial profiles of stagnation pressure 53 and 64 cm from the exit plane as well as flow angle. The impact pressure probe data compare favorably with stagnation pressures predicted by a source-flow code and suggests that the heavy particles diffuse less radially than do the electrons.

Nomenclature

A = probe surface area, m^2
A_e = nozzle exit area, m^2
A_{ki} = Einstein spontaneous emission coefficient for $k \rightarrow i$ transition
A_0 = parameter related to the formation of the boundary layer in model
A^* = nozzle throat area, m^2
e = particle charge, 1.6×10^{-19} C
g_k = degeneracy of k level
I_{ki} = spectral intensity of $k \rightarrow i$ transition
I_+ = ion saturation current, A
i_+ = dimensionless ion saturation current
k = Boltzmann's constant, 1.38×10^{-23} J/K
M_i = ion mass, kg
m_e = electron mass, 9.11×10^{-31} kg
n_e = electron number density, m^{-3}
P = plume pressure, Pa
P_b = parameter related to the expansion of the flow outside of the nozzle for model
q = dynamic pressure, Pa
r = radius from plume centerline, m
r_e = nozzle exit radius, m
r_p = langmuir probe electrode diameter, cm
T_e = electron temperature, eV
V = probe bias, V
Z_i = ion charge
β = parameter related to the density decay in the nozzle boundary layer
γ = ratio of specific heats
θ = flow angle
θ_L = limiting Prandtl–Meyer expansion angle
θ_0 = angle where the inviscid plume core meets the boundary-layer gas in the nozzle
λ_D = debye length, cm
λ_e = electron mean free path, cm
λ_i = ion mean free path, cm
λ_{ki} = wavelength of $k \rightarrow i$ transition, nm
Φ_p = plasma potential, V
χ = parameter related to the velocity decay in the nozzle boundary layer
χ_p = dimensionless probe potential

Introduction

ARCJETS currently enjoy a high degree of success, having been qualified and used for N–S stationkeeping duties on the Lockheed Martin Astro Space Series 7000 communication satellite.[1] A number of technical issues still remain to be resolved, however, if the full potential of these engines is to be realized. This is particularly true for the higher-powered arcjets that are proposed for orbit transfer and orbit maneuvering applications.[2–6] These issues include understanding how input power is parceled among the various energy modes of the working fluid, as well as how it is deposited into the arcjet structure (e.g., electrode losses), and how the transport of mass, momentum, and energy in the plume may affect spacecraft operation and lifetime.

To begin the process of characterizing transport in arcjet plumes, profiles of electron temperature, electron number density, stagnation pressure, and the flowfield were obtained over an extensive volume of a 1-kW arcjet plume. Axial and radial profile measurements were made with pressure probes and langmuir probes over a region of the plume that extends from the arcjet exit plane to over 1 m downstream. This work extends prior work[7,8] by comparing the results of langmuir probes of different sizes, characterizing the flowfield, and making detailed pressure profile measurements.

Experimental Apparatus

A 1-kW-class arcjet that was supplied by the NASA Lewis Research Center (LeRC) was used for this study.[4] The engine features a 2%-thoriated tungsten cathode and a nozzle (also of 2%-thoriated tungsten) that serves as the anode. The arcjet has a 0.51-mm-diam by 0.25-mm-long constrictor, a 30-deg half-angle converging nozzle section upstream of the constric-

Presented as Paper 94-3137 at the AIAA/ASME/SAE/ASEE 30th Joint Propulsion Conference and Exhibit, Indianapolis, IN, June 27–29, 1994; received Sept. 6, 1994; revision received May 12, 1995; accepted for publication May 12, 1995.

*Assistant Professor, Plasmadynamics and Electric Propulsion Laboratory, Department of Aerospace Engineering. Member AIAA.
†Graduate Assistant, Plasmadynamics and Electric Propulsion Laboratory, Department of Aerospace Engineering. Student Member AIAA.

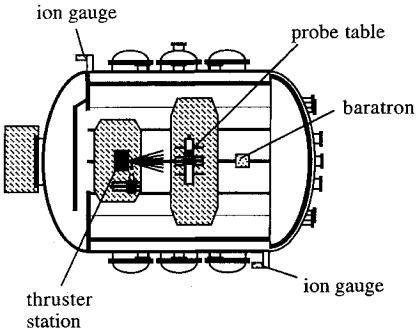

Fig. 1 Schematic of the 9 × 6 m vacuum chamber.

tor, and a 20-deg half-angle diverging section. The exit diameter of the nozzle is 9.5 mm, giving the expansion section an area ratio of 350. The electrode gap spacing is 0.51 mm. The outer housing of the device is constructed of titaniated zirconiated molybdenum (TZM).

Arcjet power is provided by a 1800-W Sorensen power supply conditioned by a NASA LeRC power processing unit (PPU). The PPU nominally operates at output voltages between 100–120 V at currents between 6–12 A with ±1.5-A ripple.[9]

Arcjet voltage is measured with Tektronix P6007 ×100 voltage probes that are clamped to the electrode leads. The voltage probe signals are collected by a Tektronix AM501 operation amplifier. Digital multimeters are used to measure the discharge voltage as well. Arcjet current is monitored with a Tektronix A6303 current sensor powered by a Tektronix AM503 current probe amplifier. Arcjet voltage and current data are monitored and stored by the computerized data acquisition system described later.

All experiments reported were performed in a 9-m-long by 6-m-diam stainless-steel vacuum chamber (Fig. 1). The facility is supported by six 81-cm-diam diffusion pumps (with water-cooled coldtraps) rated each at 32,000 l/s on nitrogen, backed by two 2000-cfm blowers, and four 400-cfm mechanical pumps. These pumps give the facility an overall pumping speed of over 180,000 l/s at 10^{-5} torr. In addition, a Polycold PFC-1100 closed-loop water cryopump has been installed to double the water pumping speed of the facility to over 150,000 l/s. This greatly reduces the pumpdown time needed for the facility. It typically takes 4 h to evacuate the chamber to 3×10^{-5} torr from atmospheric pressure.

Chamber pressure is measured with MKS model 919 hot-cathode ionization gauges, that were corrected for hydrogen, located on vacuum ports on either side of the chamber, and by an MKS type 317HA Baratron capacitance manometer located in the center of the chamber. Background chamber pressure is maintained to 4×10^{-4} torr (0.053 Pa) or less when the arcjet is operating on 15 mg/s of pure hydrogen.

Propellant is supplied to the arcjet from compressed gas bottles through stainless-steel feed lines. Hydrogen propellant flow is controlled and monitored with an MKS 1159B mass flow controller that is specially calibrated for light gases. The system is capable of providing up to 16 mg/s of hydrogen with an accuracy of 1%. The flow controller is periodically calibrated with a calibration rig that measures gas pressure and temperature as a function of time in an evacuated chamber of known volume. These data are then used to estimate the mass flow rate via the ideal gas equation of state.

A Macintosh-based data-acquisition system (Labview) monitors all thruster, diagnostics, and tank operations. The system includes 32 isolated differential input channels that are used in conjunction with a high-speed data acquisition board, and a high-speed IEEE-488.2 (GPIB) interface card. The interface card allows for the ability to control instruments with GPIB communication ports.

Plume diagnostics, both in the near and farfields, were performed through the use of a custom-made probe positioning system. The table contains two rotary platforms on a 1.8-m-long linear stage mounted radially on a 0.9-m travel axial stage. The rotary actuators not only allow langmuir and pressure probes to be rotated to minimize measurement errors due to probe misalignment with the flow,[10–13] but also for the purpose of characterizing the local flowfield. The system allows for sweeps with two probe rakes at radial speeds in excess of 60 cm/s with an absolute position accuracy of 0.15 mm. The system is operated by its own Macintosh-driven control station via Labview software. Like the thruster station, the entire probe positioning system is mounted on a movable platform to allow for measurements to be made throughout the chamber (Fig. 1).

Spectroscopic measurements were made with a Spex Industries model 500M Czerny–Turner type spectrometer. The spectrometer has a focal length of 0.5 m and an *f*/4 aperture. A 1800 g/mm holographic grating, blazed at 500 nm, was used for all measurements, giving the spectrometer a dispersion of 1.2 nm/mm, a spectral range between 120–1000 nm, and a wavelength resolution of 0.015 nm. Light detection is achieved using a Hamamatsu R928 photomultiplier tube (PMT) powered by a Spex-35870-1 high-voltage power supply. High voltage to the PMT is computer controlled, and spectrometer scans are monitored, controlled, and stored on a 486 personal computer. A Stanford Research SR850 dual phase digital lock-in amplifier, in conjunction with a chopper, is used to provide phase-sensitive spectrometer scans.

Because of the large size of the chamber, direct optical access to the exit of the thruster is difficult to achieve. Thus, light from the arcjet plume is focused onto the face of a 100-μm-diam silica optical fiber by a 25-mm-diam achromatic lens within the chamber, and is transmitted to the spectrometer via a vacuum feedthrough. The exiting light from the optical fiber is then focused onto the entrance slit of the spectrometer by another achromatic lens.

To allow radial scans to be made at or near the arcjet exit plane, the collection optics are mounted on a 28-cm-travel personal computer-controlled linear positioning table mounted vertically to the side of the thruster station next to the arcjet. This allows the collection optics to be positioned approximately 10 cm above or below the center of the plume. When not in use, the collection lens is stored in a safe-box at the top of the stage to protect it from the plume.

Characterization of the spectral response for this imaging system was made using a tungsten lamp in place of the arcjet plume. Emissivity values for tungsten were used to determine the actual spectral output of the lamp. True lamp intensity along with the corresponding measured intensity acquired from the spectrometer PMT signal was then used to determine the system's spectral response. The spectral response function was used to correct the measured intensity at a given wavelength to its true value.

Results and Discussion

All near- and far-field arcjet measurements were made with the arcjet operating on pure hydrogen at a mass flow rate of 15 mg/s (10 standard liters per minute), at a current of 10 A, and a voltage of approximately 110 V. Chamber pressure was maintained at 4×10^{-4} torr or less during all tests. At this pressure, the mean free path of the background gas is approximately 35 cm.[14] The arcjet was allowed to run for a 20-min warm-up period after ignition before measurements were made to ensure that the engine had reached thermal equilibrium (i.e., once the arcjet voltage reached its steady-state value). At this operating condition, current and voltage ripple were measured with a digital oscilloscope to be approximately ±1.4 A and ±6 V, respectively, at a frequency of 18 kHz. These characteristics are well within the nominal operating parameters of the PPU.[9]

Near-Field Langmuir Probe Measurements

A cylindrical single langmuir probe was used to measure n_e and kT_e near the exit of the arcjet. The probe is composed of a tungsten wire electrode, 0.23 mm in diameter by 1.9 cm long, attached to the center conductor of a titanium triaxial boom with Teflon® insulation. The boom is approximately 4 mm in diameter by 18 cm long.

The collector electrode of the probe was biased with respect to the chamber wall by a programmable bipolar power supply. A function generator was used to provide the input 12.7-Hz triangular waveform that was amplified to ± 10 V by the bipolar supply. Since the arcjet anode is tied to chamber ground, there is no need to use an isolation transformer to power the bipolar supply.

Probe current, as determined via a 10-Ω shunt, and probe voltage, referenced with respect to tank ground, were measured with voltage probes. Shunt and voltage probe output signals were collected both by the data acquisition system and the digital oscilloscope. The data acquisition system stored 50 pairs of probe voltage–current data samples per voltage ramp.

All near-field measurements were made with the tip of the langmuir probe placed 20 mm downstream of the nozzle exit. To collect data this close to the exit without overheating the probe, the probe was quickly moved to the collection site (at the appropriate angle), kept there long enough to collect 10 ramps of data (~1 s), and rapidly moved out of the plume to allow for probe cooling. This approach also served as an effective means of cleaning the probe since the probe electrode was observed to glow as it was removed from the plume.

Since $r_p/\lambda_D \geq 10$ and $\lambda_i/r_p > 100$ in the near-field region of the plume, the standard collisionless thin sheath Bohm ion saturation current model was used to interpret langmuir probe data. To account for ion current collection due to convection from the flowing plasma, the probe angle was varied between 0–10 deg with respect to the plume axis of symmetry. This probe rotation range was selected because at angles greater than 10 deg, the boom of the probe was observed to perturb the flow significantly.

Figure 2 shows radial electron temperature and number density profiles. As the figure shows, electron number density measurements are quite sensitive to probe angle. The peak value of n_e (slightly offset from the axis) at 10 deg is more than twice that with the probe aligned with the thruster axis. However, the n_e data for the three probe orientations converge with increasing radius and identical values are predicted 18 mm from the centerline. Laser induced fluorescence (LIF) measurements have shown the axial velocity of hydrogen arcjets to decrease rapidly with radius.[15] Thus, the fact that probe angle has little influence on number density measurements at this location may be an indication that the local flow velocity is close to the heavy particle thermal speed, and so convective ion collection at the probe becomes indistinguishable from random flux collection.[10]

Higher-than-expected electron temperatures were measured with the langmuir probe (Fig. 2). Electron temperature is seen to decrease with increasing probe angle, but to remain relatively constant with radius. This last trend has been observed in higher-powered hydrogen arcjets (10 kW) via emission spectroscopy.[16] Only the 10-deg probe data predict expected values of T_e. The reason for this probe angle dependence is not known at this time.

Emission Spectroscopy

Data were taken by translating the optics in 1-mm increments perpendicular to the plume axis 12 mm downstream of the exit plane and 15 cm to the side of the arcjet centerline. The spectrometer entrance slit was set at 100 μm to maximize the amount of light collected by the spectrometer, while the exit slit was set at 500 μm to ensure capture of Stark broadened hydrogen lines. The emissivity coefficient for each measured transition was then calculated from intensity profiles along various chords of the plume via Abel inversion. With the emissivity coefficient, Boltzmann plots were then made to determine the electron temperature as a function of radius.

Figure 3a shows examples of Boltzmann plots made at three radial locations, 12 mm downstream of the exit plane. The 434-, 410-, and the 397-nm Balmer lines were used for this plot. The linearity of this plot suggests that the upper states used in the Boltzmann plot are in local thermal equilibrium with the electrons and can be used to measure electron temperature, a conclusion reached in other arcjet studies.[17]

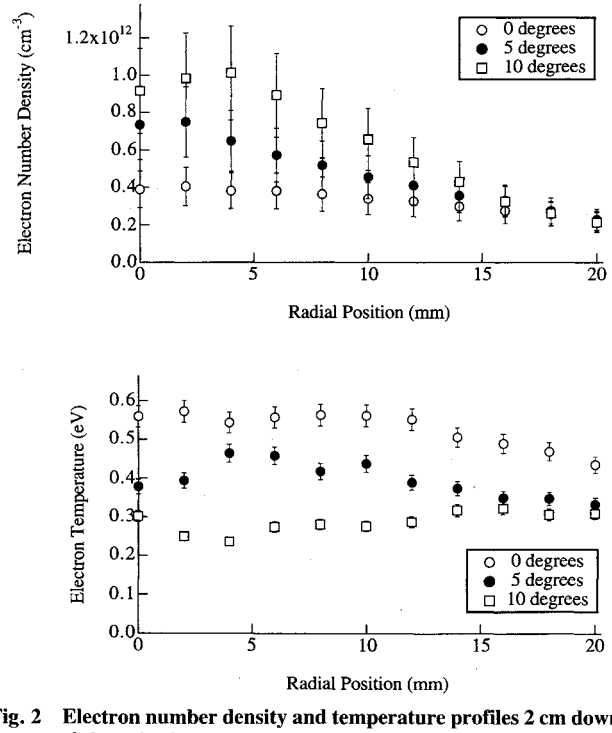

Fig. 2 Electron number density and temperature profiles 2 cm downstream of the exit plane.

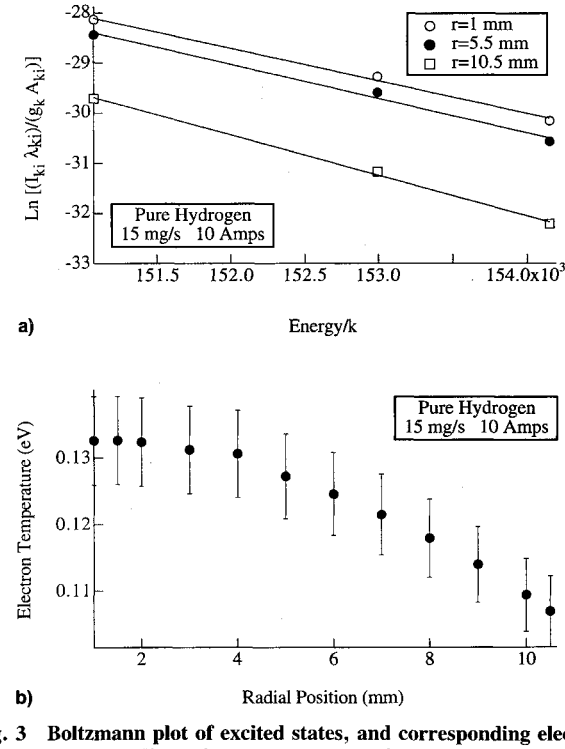

Fig. 3 Boltzmann plot of excited states, and corresponding electron temperature vs radius 1.2 cm downstream of the exit plane.

Figure 3b plots electron temperature, determined from the Boltzmann plot, as a function of radial position. As the figure shows, the electron temperature drops off rapidly with radius. The peak electron temperature of ~0.13 eV is found near the center of the plume. At 10.5 mm from the plume center, the electron temperature drops to less than 0.11 eV. Initially, four hydrogen Balmer lines were used in this study for making Boltzmann plots, the 486-, 434-, 410-, and the 397-nm lines. It was observed, however, that the electron temperatures predicted with these Boltzmann plots increased with radius, a trend that is counterintuitive. This behavior suggests that the low-lying states on the plot may not be in equilibrium with the electron energy distribution.

The 486-nm state lies 0.31 eV below the nearest upper exited state in the Balmer series. As a consequence of the wide (relative to T_e) energy spacing between this state and its nearest upper excited state, it is improbable that the electrons are in equilibrium with it. Additionally, the intensity of this state decreases with radius as the true electron temperature and density decreases, and as the lower-lying excited states in general fall further out of equilibrium. This results in a flattening of the slope of the Boltzmann line at large radii, resulting in artificially high T_e. This low-lying state was thus removed to make Fig. 3a, and the data were refitted to predict the electron temperature profile shown in Fig. 3b. The electron temperatures calculated from the corrected Boltzmann plot are consistent with the energy spacing between these upper states. This finding suggests that the upper states used in Fig. 3a are in local thermal equilibrium with the electrons and can be used to measure electron temperature. Since the Einstein spontaneous emission coefficients for hydrogen are precisely known, the error associated with the electron temperatures obtained from the Boltzmann plot are estimated to be approximately 5%.[18]

Of concern is the disagreement between the langmuir probe and spectroscopy T_e data. The source of this discrepancy is unknown at this time; however, future experiments will be performed to resolve this issue.

Far-Field Langmuir Probe Measurements

To measure electron temperatures and densities approximately 1 m from the arcjet exit plane, where λ_D is on the order of 0.1 mm,[7] a 0.42-cm-diam by 5.1-cm-long cylindrical rhenium langmuir probe was used in conjunction with the smaller probe used for near-field single-probe measurements. The collector electrode was formed by vapor-depositing rhenium on a molybdenum mandrel.

In the far field, λ_e and λ_i are expected to be an order of magnitude larger than the diameter of the large probe and at least two orders of magnitude larger than the sheath. Furthermore, since r_p/λ_D will be approximately 20 or more for the large probe, a thin sheath saturation current model was used to analyze data from this probe. The probe was cleaned with acetone prior to each test.

Figure 4 shows profiles of electron temperature and number density as measured with the large probe using the thin sheath model. The probe angle was rotated to 0, 5, 10, 20, and 30 deg with respect to the thruster axis at each location. The probe was moved continuously at a radial speed of 1.2 cm/s. Thus, 50 pairs of probe voltage–current data points were collected per millimeter of radial travel (i.e., per voltage ramp). A Hewlett–Packard workstation running Matlab was used to process the tens of thousands of data points to obtain electron temperatures and number densities. Only data collected at angles for which the axis of the probe is aligned with the local flow (i.e., minimum ion saturation current) are reported.

As the figure shows, the peak number density drops from 5×10^9 to less than 2×10^9 cm^{-3} over a 58 cm increase in axial position. At 30 cm from the exit, the number density at the edge of the measurement region is nearly an order of magnitude smaller than the peak value. At the 88-cm position,

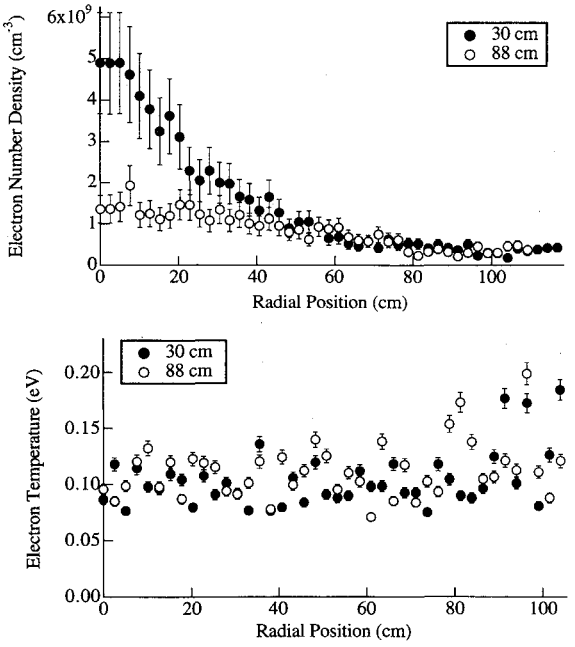

Fig. 4 Electron number density and temperature profiles at axial positions 30 and 88 cm from the exit plane.

the radial electron number density profile is flat, suggesting that the exhaust rapidly assumes a uniform spherical expansion pattern. This conclusion is justified by examining flow angle data from impact pressure probe measurements described later. The variation in electron temperature, however, is not nearly so dramatic, and is approximately 0.1 eV at both axial locations. The increased scatter and higher indicated temperature at the fringe of the measurement region may be due to probe misalignment with the flow.

To interpret data from the small probe in the far field where $r_p/\lambda_D \simeq 1$, an ion saturation current model from Laframboise[19] was used. This model is accurate for cylindrical langmuir probes in quiescent plasmas devoid of magnetic fields, where $r_p/\lambda_D < 2.5$ (Ref. 19):

$$I_+^2 = (2e^3 n_e^2 A^2/\pi^2)(Z_i/M_i)(\Phi_p - V) \tag{1}$$

It should be noted that in contrast to the Bohm thin sheath model, in this limit the ion saturation current no longer depends on electron temperature.

To test the validity of the model, the ion saturation current of the small probe was measured as a function of probe potential in a portion of the arcjet plume where the electron temperature and number density had been measured at ~0.1 eV and 1×10^9 cm^{-3} by the large probe. The probe was placed along the center of the plume both parallel and perpendicular to the axis of the arcjet. These data are shown on Fig. 5, which plots dimensionless ion saturation current, defined by

$$i_+ = i_+/\{en_e A[Z_i kT_e/(2\pi M_i)]^{1/2}\} \tag{2}$$

vs dimensionless probe potential:

$$\chi_P = e(V - \Phi_p)/kT_e \tag{3}$$

Also plotted are Laframboise's models for $r_p/\lambda_D < 2.5$ [Eq. (1)] and for $r_p/\lambda_D = 3.5$.[19] As the figure shows, the Laframboise model for the case of $r_p/\lambda_D < 2.5$ is in excellent agreement with the small probe data, where $r_p/\lambda_D \simeq 1.5$. The figure also shows that slightly higher saturation currents are measured when the probe is perpendicular to the local ion flow, as expected.

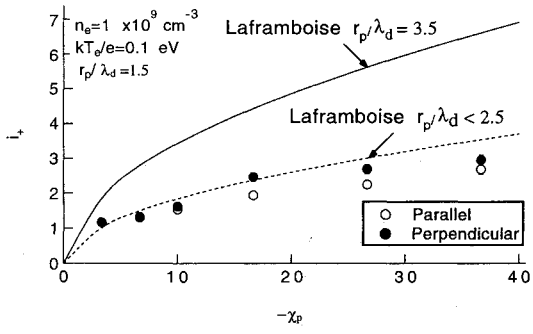

Fig. 5 Normalized ion current vs probe potential.

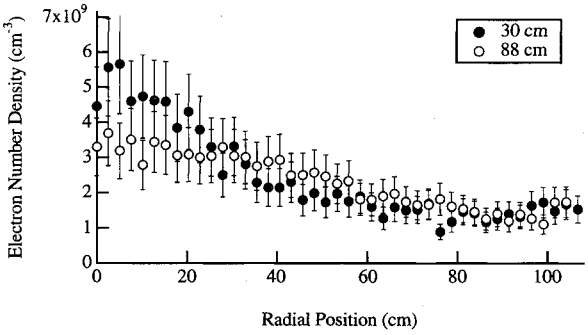

Fig. 6 Electron number density profiles at axial positions 30 and 88 cm from the exit plane.

Partially corrected number density data from the small probe are plotted on Fig. 6. The partial correction made to the data includes using large-probe electron temperature data with a Bohm model. This adjustment is necessary since T_e values calculated from the small probe assuming Bohm current collection were approximately an order of magnitude too high (~1 eV). Although the source of this error is thought to be due to the erroneous model used, no attempt was made to incorporate Laframboise's models in calculating T_e or n_e with the small probe at this time. The fact that the peak number density in Fig. 6 is offset from the 0-cm radial position may be an indication that the probe axis is slightly misaligned with the thruster centerline.

Using the Bohm model, the data from the small probe tend to be flatter in profile than those from the large probe, and tend to overpredict n_e throughout the plume. The overprediction in n_e at the region of the plume of lowest density is expected, since finite sheath thickness effects are expected to have a significant impact on current collection. In fact, this phenomenon can be exploited as a diagnostic. By using the electron temperatures and number densities measured with the large probe in conjunction with the saturation currents measured with the small probe, an estimate of the sheath thickness can be made by calculating the effective collection area of the small probe. Preliminary calculations to this effect have found that the effective collection area of the small probe is approximately 2.5 times that of the actual probe surface, in the case of $r_p/\lambda_D \simeq 1.5$. This suggests that the radius of the collection cylinder is $\sqrt{2.5}$ times r_p and that the sheath thickness is $0.6r_p$. Since $\lambda_D/r_p \simeq 1/1.5 = 0.67$, the sheath that forms on the small probe is approximately 1 D length thick.

Far-Field Pressure Measurements

The task of measuring plume pressures in a supersonic rarefied flow represents several challenges. In flows with Knudsen numbers of order one (transitional flows), particle interactions with the probe structure, in terms of heat transfer and scattering, can profoundly affect measured pressures.[20-24] These nonequilibrium effects often render pressure data from poorly designed pressure probes useless. To investigate this effect, an impact probe was designed and placed in the far-field plume of the arcjet. The probe (Fig. 7) consists of a 10-cm-long by 1.3-cm-o.d. aluminum tube, with a 10-deg entrance lip, attached to an MKS model 627 Baratron capacitance manometer. This pressure sensor was calibrated to a pressure of 1×10^{-4} torr. The purpose of the 10-deg chamfer is to minimize edge effects at the collection orifice by ensuring that most incident particles are directed to the pressure measuring volume of the sensor.[13]

Output from the Baratron was processed with an MKS PDR-C-1C display and the data acquisition system. The probe assembly was connected to a boom that was placed on the probe positioning system. Through use of the theta table, the probe could be rotated to more than ±90 deg from the thruster axis.

Figure 8 shows typical theta scan data from −90 to 90 deg, with the probe at a fixed spatial location approximately 0.5 m from the nozzle exit. The local flow angle can be interpreted

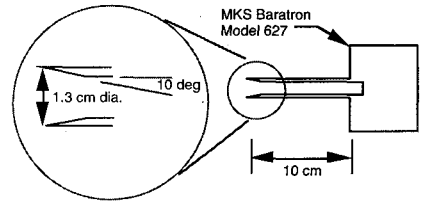

Fig. 7 Detail of the impact pressure probe assembly showing 10-deg internal chamfer on probe lip.

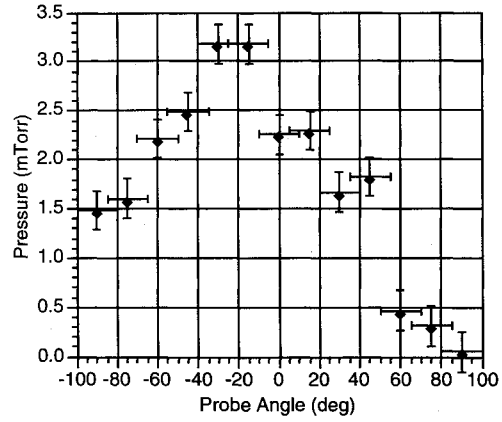

Fig. 8 Impact probe pressure vs probe angle for data taken 48 cm downstream of the exit plane and 25 cm radially from the plume center.

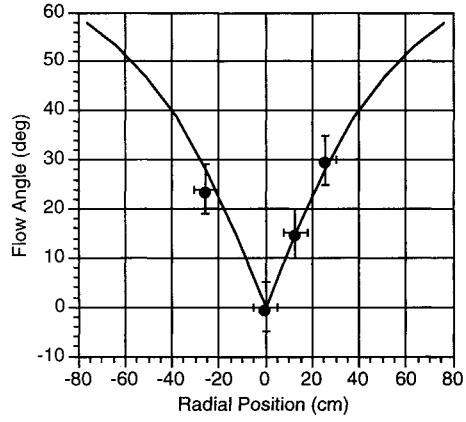

Fig. 9 Flow angle, as determined from impact probe measurements, vs radial position 25 cm downstream of the exit plane. Solid curve represents source flow model prediction.

as the point corresponding to the maximum pressure reading (i.e., when the probe is pointed directly into the oncoming flow). The figure shows that the local flow angle at this spot is approximately 20 deg with respect to the thruster axis. This process can be repeated at various axial and radial locations to map the local flowfield in terms of direction. An example of this is shown in Fig. 9, which shows flow angle as a function of radial position 25 cm downstream of nozzle exit. Flow angle at each spot is determined from recording the angle of maximum pressure when the probe is rotated through 180 deg at a fixed spatial location. The curve on this figure shows flow angle as computed from the source flow model described later. As expected, the flow angle of the expanding plume increases with radial position. Although few points are reported, the fact that the data corroborate the source flow code and are symmetric about the thruster centerline (0 cm position) is especially encouraging.

Although it has been demonstrated that this technique can be used to map qualitatively the far-field flow pattern, it was of particular interest to determine if absolute pressure measurements could be made. To this effect, the Revised Plume Model (RPM) code[25] was used to generate dynamic pressure simulations of the arcjet plume. The code is capable of generating a complete spatial flowfield map of dynamic pressure values for a nozzle exhausting into vacuum. The input parameters for the code include nozzle geometry, stagnation pressure and temperature, molecular weight, γ, and the boundary-layer thickness at the nozzle exit.

The RPM code was written with the goal of obtaining an accurate model of the Shuttle Orbiter's Primary Reaction Control System (PRCS) nozzle plumes.[25] The code has been ground verified and modified using conventional cold gas expansion nozzles in a large vacuum chamber. No attempt was made at modifying the code for arcjet plumes.

Since the ionization fraction of the plume is low ($<10^{-2}$), a high-temperature neutral gas mixture of 30% dissociated hydrogen was assumed for the model. This level of dissociation was estimated by assuming the flow to be in chemical equilibrium in the constrictor and frozen throughout the nozzle. Thus, the very small amount of ionization in the plume combined with the simple nozzle geometry should create a plume flowfield that is similar to that of a conventional rocket with a high exhaust temperature.[26] Successful extension of conventional plume flowfield solvers such as RPM to the plume of arcjets provides a simple method of predicting the flow of the neutral species from these devices. This application, if successful, would eliminate the need for development of costly arcjet solvers employing complicated (and unnecessary) models to account for chemistry in the plume.

The RPM code is based on a source flow model in that the neutral gas species are assumed to behave as though they were emitted from a supersonic point source located at the nozzle exit plane. The density of this flow is assumed to fall off as $1/r^2$ in the inviscid core of the plume to satisfy mass conservation. An exponential decay factor is applied to the gas originating from the nozzle boundary layer, giving for q:

$$q = A_0 P_b \frac{A^*}{A_e}\left(\frac{r_e}{r}\right)^2 \frac{\gamma}{\gamma-1}\left(\frac{2}{\gamma+1}\right)^{1/(\gamma-1)} \xi(\theta) \qquad (4)$$

For $\theta < \theta_0$

$$\xi(\theta) = \left[\cos\left(\frac{\pi}{2}\frac{\theta}{\theta_L}\right)\right]^{2/(\gamma-1)} \qquad (5)$$

For $\theta_0 \le \theta \le \pi$

$$\xi(\theta) = \left[\cos\left(\frac{\pi}{2}\frac{\theta}{\theta_L}\right)\right]^{2/(\gamma-1)} \exp[-(\beta + 2\chi)(\theta - \theta_0)] \qquad (6)$$

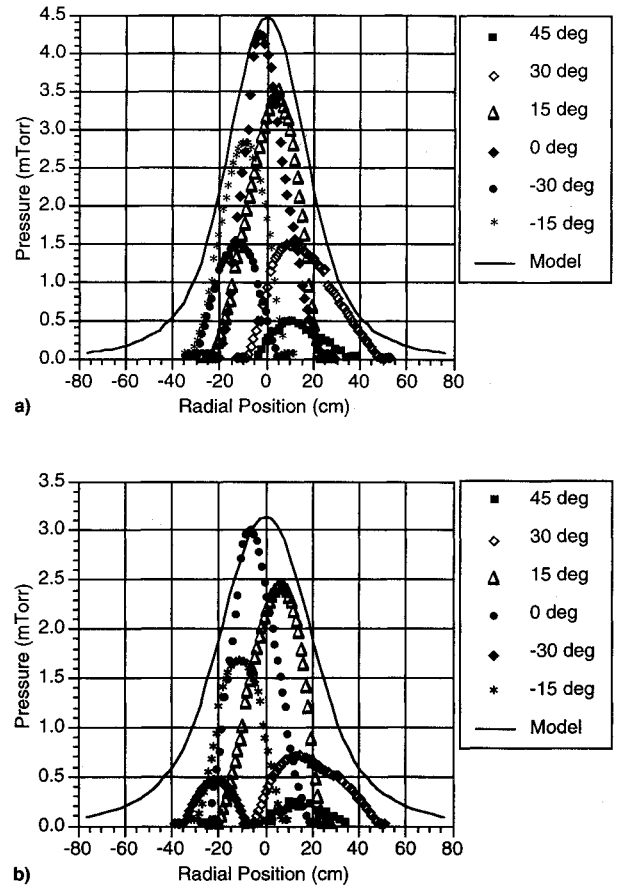

Fig. 10 Impact pressure probe data at various angles vs radial position at axial positions a) 53 and b) 64 cm from the exit plane.

This model is expected to be most accurate within 60 deg of the thruster axis.[26,27]

Figure 10 shows comparisons between dynamic pressure profiles predicted by the code and impact pressure probe data at two axial locations (53 and 64 cm from the nozzle exit). As model inputs, the arcjet boundary-layer thickness was estimated to be 1 mm at the exit, based on a simple boundary-layer analysis, and the stagnation temperature and pressure were set to 3300 K and 0.27 MPa, respectively. Temperature and pressure inputs were determined from experimental data.[4,15] Data points represent radial sweeps at discrete probe angles across the entire radial table (150 cm long) within a 50-deg cone from the nozzle. As the figure shows, at each axial location the envelope of data is enclosed in the profile predicted by the model. The model predicts higher pressures near the ends of the table (± 30 in.) than are measured. For these measurements, uncorrected tank pressure was recorded at 1.4×10^{-4} torr with the side-mounted ionization gauges. Thus, the fact that dynamic and static pressure at the edge of the measurement region fall below the lower limit detectable by the Baratron (10^{-4} torr) not only corroborates ionization gauge data, but suggests that the bulk of the neutrals flows within 50 cm of the plume center at these axial locations. Lastly, by comparing measured pressures with measured electron temperatures and number densities at these axial positions, and by assuming a heavy particle translational temperature of 2000 K, an upper limit to the on-axis neutral gas density was calculated to be $\sim 10^{13}$ cm^{-3}, corresponding to an ionization fraction of $\sim 10^{-4}$.

Conclusions

A detailed study of the plume of a 1-kW hydrogen arcjet has been performed using langmuir probes, impact pressure

probes, and emission spectroscopy. In the near-field region, analysis of the hydrogen Balmer lines suggests that only the upper three states of that series are in local thermodynamic equilibrium with the electrons, and use of lower states could result in erroneous temperature measurements. Near-field langmuir probe measurements at varying probe angles suggest that the axial flow velocity 20 mm downstream of the nozzle exit varies rapidly with radius, and at 20 mm from the centerline the exhaust plume may be near the local heavy particle thermal speed.

The langmuir probe was found to predict accurately far-field number densities using the Bohm saturation model when its radius is much larger than the local debye length. An ion saturation current model from Laframboise was found to account accurately for finite sheath effects that are present when the probe dimensions are on the order of the debye length. By using saturation current data from two probes of different sizes, it was concluded that the sheath thickness near the probe in the plume is approximately 1 D length.

Comparison of impact pressure probe measurements with a source-flow model was favorable. It was demonstrated that flowfield information could be obtained from these measurements and that a relatively simple instrument could be used to measure dynamic pressure. By incorporating measured electron temperatures, number densities, and an assumed heavy particle temperature with these pressure data, the ionization fraction was estimated to be 10^{-3} or less.

Acknowledgments

This work was supported through Grants from NASA LeRC, NASA JSC, and the University of Michigan Office of the Vice President for Research. The authors would like to thank Shawn Ohler for help in analyzing far-field data, Colleen Marrese for general "VI" development, and Mark Reichenbacher for writing software sequences for the probe positioning system. The authors would also like to thank the technical support staff of the Aerospace Engineering Department for their help in maintaining the facilities, NASA LeRC and JSC for instrumentation support, Arnaud Turlan of ENSICA (France) for data processing, and Larry Brace of the University of Michigan Space Physics Research Laboratory for use of his langmuir probes.

References

[1]Smith, R. D., Yano, S. E., Lichtin, D. A., and Beck, J. W., "Flight Qualification of a 1.8 kW Hydrazine Arcjet System," IEPC-93-007, Sept. 1993.

[2]Sneegas, S. A., Rosenthatl, R. A., and Vondra, R. J., "Space Surveillance Track and Autonomous Reposition (SSTAR) Experiment," IEPC-93-054, Sept. 1993.

[3]Sutton, A. M., "Overview of the Air Force ESEX Flight Experiment," IEPC-93-057, Sept. 1993.

[4]Sankovic, J. M., Hamley, J. A., Haag, T. W., and Curran, F. M., "Hydrogen Arcjet Technology," IEPC-91-018, Oct. 1991; also NASA TM-105340, Oct. 1991.

[5]Curran, F. M., Bullock, S. R., Haag, T. W., Sarmiento, C. J., and Sankovic, J. M., "Medium Power Hydrogen Arcjet Performance," AIAA Paper 91-2227, June 1991; also NASA TM-104533, June 1991.

[6]Pivirotto, T., King, D., Deninger, W., and Brophy, J., "The Design and Operating Characteristics of a 30 kW Thermal Arcjet Engine for Space Propulsion," AIAA Paper 86-1508, June 1986.

[7]Carney, L. M., and Sankovic, J. M., "The Effects of Arcjet Thruster Operating Conditions and Constrictor Geometry on the Plasma Plume," AIAA Paper 89-2723, July 1989; also NASA TM-102285, July 1989.

[8]Pencil, E. J., Sarmiento, C. J., Lichtin, D. A., Palchefsky, J. W., and Bogorad, A. L., "Low Power Arcjet System Spacecraft Impacts," AIAA Paper 93-2392, June 1993.

[9]Gruber, R. P., "Power Electronics for a 1-Kilowatt Arcjet Thruster," AIAA Paper 86-1507, June 1986; also NASA TM-87340, June 1986.

[10]Tilley, D. L., Gallimore, A. D., Kelly, A. J., and Jahn, R. G., "The Adverse Effect of Ion Drift Velocity Perpendicular to a Cylindrical Triple Probe," *Review of Scientific Instruments*, Vol. 65, No. 3, 1994, pp. 678–681.

[11]Steckelmacher, W., and Lucas, M. W., "Gas Flow Through a Cylindrical Tube Under Free Molecular Conditions," *Journal of Physics D: Applied Physics*, Vol. 16, 1983, pp. 1453–1460.

[12]Meyer, J. T., "Free Molecular Pressure Measurements in the Continuum, Transitional, and Free Molecular Regimes of a Free Jet," *Rarefied Gas Dynamics: Proceedings of the 17th International Symposium* (Aachen, Germany), VCH Verlagsgesellschaft, mbH, 1990, pp. 963–970.

[13]Koppenwallner, G., "The Free Molecular Pressure Probe with Finite Length Slot Orifice," *Rarefied Gas Dynamics: Proceedings of the 14th International Symposium* (Tsakuba, Japan), Univ. of Tokyo Press, Japan, 1984, pp. 415–422.

[14]Dickerson, R. E., Gray, H. B., Haight, G. P., Jr., *Chemical Principles*, 3rd ed., Benjamin/Cummings Publishing Co., Inc., Menlo Park, CA, 1979, p. 128.

[15]Liebeskind, J. G., Hanson, R. K., and Cappelli, M. A., "Flow Diagnostics of an Arcjet Using Laser-Induced Fluorescence," AIAA Paper 92-3243, July 1992.

[16]Hoskins, W. A., "Measurement of Population and Temperature Profiles in an Arcjet Plume," AIAA Paper 92-3240, July 1992.

[17]Zube, D. M., and Myers, R. M., "Thermal Nonequilibrium in a Low-Power Arcjet Nozzle," *Journal of Propulsion and Power*, Vol. 9, No. 4, 1993, pp. 545–552.

[18]*CRC Handbook of Chemistry and Physics*, 69th ed., edited by R. C. Weast, CRC Press, Boca Raton, FL 1989, p. E337.

[19]Laframboise, J., "Theory of Cylindrical and Spherical Probes in a Collisionless Plasma at Rest," *Rarefied Gas Dynamics*, Vol. 2, edited by J. H. deLeeuw, Academic, New York, 1966, pp. 22–44.

[20]Wainwright, J. B., and Rogers, K. W., "Impact Pressure Probe Response Characteristics in High Speed Flows with Transition Knudsen Numbers," Univ. of California Eng. College Rept. 101-101, 1964.

[21]Potter, J. L., Kinslow, M., and Boylan, D. E., "An Influence of the Orifice on Measured Pressures in Rarefied Flow," *Rarefied Gas Dynamics: Proceedings of the 4th International Symposium*, Arnold Engineering Development Center, 1966, pp. 175–194.

[22]Hughes, P. C., "Theory for the Free Molecule Impact Probe at an Arbitrary Angle of Attack," Univ. of Toronto, Inst. for Aerospace Studies, Rept. 103, Toronto, ON, Canada, 1965.

[23]DeLeeuw, J. M., and Rothe, D. E., "A Numerical Solution for the Free Molecule Impact Pressure Probe Relations for Tubes of Arbitrary Length," Univ. of Toronto, Inst. for Aerospace Studies, Rept. 88, Toronto, ON, Canada, 1962.

[24]Pond, M. L., *Journal of Aerospace Sciences*, Vol. 29, 1962, pp. 917–920.

[25]Fitzgerald, S. M., Bouslog, S. A., and Hughes, J. R., "Model for Predicting Orbiter PRCS Plume Impingement Loads," NASA JSC-26507, Jan. 1994.

[26]Simons, G. A., "Effect of Nozzle Boundary Layers on Rocket Exhaust Plumes," *AIAA Journal*, Vol. 10, No. 11, 1972, pp. 1534, 1535.

[27]Bird, G. A., "Breakdown of Continuum Flow in Freejets and Rocket Plumes," *Rarefied Gas Dynamics*, Vol. 74, Pt. II, Progress in Astronautics and Aeronautics, AIAA, Washington, DC, 1981.